PHILOSOPHICAL TRANSACTIONS OF THE ROYAL SOCIETY A MATHEMATICAL, PHYSICAL & ENGINEERING SCIENCES

Inertial cavitation and single–bubble sonoluminescence

Thomas J. Matula

Phil. Trans. R. Soc. Lond. A 1999 **357**, 225-249
doi: 10.1098/rsta.1999.0325

THE ROYAL SOCIETY

Inertial cavitation and single-bubble sonoluminescence

By Thomas J. Matula

Applied Physics Laboratory, University of Washington, 1013 NE 40th St., Seattle, WA 98105, USA

Sonoluminescence is investigated experimentally from the perspective of the dynamics of a single inertial cavitation bubble levitated in an acoustic sound field. The discussion includes bubble levitation, the inertial cavitation threshold, the parameter space in which stable single-bubble sonoluminescence is observed, measurements of the acoustic and electromagnetic emissions from a sonoluminescence bubble, and the effects of impurities on the quality of the light emission from sonoluminescence bubbles. Comparisons are also made between sonoluminescence from a single bubble and sonoluminescence from a cavitation field.

Keywords: bubble dynamics; bubble levitation; cavitation; sonoluminescence; single-bubble sonoluminescence; light emission

1. Introduction

Acoustic cavitation—the sequence of formation, growth and collapse of a vapour or gas bubble—can lead to an enormous concentration of energy (evaluated by some to be as high as 12 orders of magnitude). The temperatures and pressures experienced by the material contained within the imploding cavities can achieve values in excess of thousands of degrees and tens of kilobars, respectively. These high temperatures and pressures can act as an intense microreactor to induce a variety of chemical reactions within and surrounding (through secondary reactions) the bubble. Under certain conditions, the energy concentration is sufficient to generate light emission, termed sonoluminescence, from within the bubble.

In this paper we will examine acoustic cavitation from the perspective of a single bubble undergoing extremely nonlinear pulsations, and the associated sonoluminescence from a single bubble, termed single-bubble sonoluminescence (SBSL). A related phenomenon involves cavitation from a field of bubbles, and the sonoluminescence from such a cavitation field is termed multibubble sonoluminescence (MBSL). We will emphasize the relatively simple system of a single stable cavitating bubble, although we touch upon the relation of SBSL to MBSL towards the end.

The remarkable properties associated with SBSL include the transduction of acoustic energy into light energy with a very short emission lifetime (Gompf *et al*. 1997; Hiller *et al*. 1998), an optical spectrum that is smooth and increasing into the ultraviolet (Hiller *et al*. 1992; Hiller 1995), and remarkably stable bubble dynamics over thousands of acoustic cycles (Barber *et al*. 1992). Such observed properties have led to an abundance of theories to explain the mechanism behind sonoluminescence. Our focus is on sonoluminescence as it relates to the dynamics of a cavitation bubble; this is not intended to be a review of sonoluminescence (which is changing at a rapid pace). For the interested reader, a review of various aspects of SBSL is given in Barber *et al*. (1997).

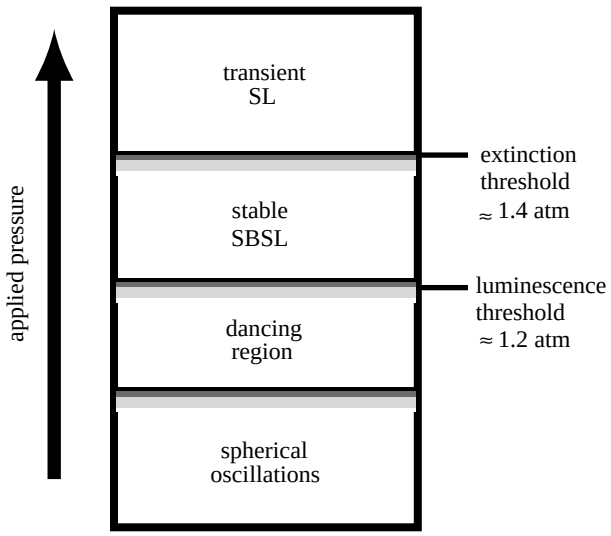

Figure 1. The drive-pressure parameter space for bubbles in an acoustic standing wave. At low drive pressures the bubble oscillates linearly, but dissolves. As the drive-pressure amplitude is increased the bubble oscillates in a nonlinear unstable fashion. Increasing the drive pressure further results in the bubble 'locking into place', and corresponds to crossing the incipient luminescence threshold. Sonoluminescence occurs between the luminescence and extinction threshold. Above the extinction threshold only a transient occurrence of the bubble is observed.

2. Parameter space

We limit this discussion of cavitation to regions in the parameter space that include stable SBSL. This includes a frequency between about 10 and 50 kHz, with an ambient bubble radius of about 1–10 μm; thus the bubble is driven below its linear resonance frequency. SBSL is found to occur over a relatively small region of drive-pressure amplitudes. Figure 1 illustrates the various regions in acoustic pressure-amplitude space under the conditions stated above. At low driving pressures, the bubble oscillates in a spherical manner, but dissolves due to surface tension. At higher drive pressures, the bubble grows by rectified diffusion (Crum 1980) and eventually fragments and reforms; micro-jetting, surface instabilities and dancing behaviour are observed (Holt & Gaitan 1996). As the drive-pressure amplitude is increased further, one notices that the bubble appears to 'lock' in place. This stability is typically coincidental with light emissions, i.e. the incipient sonoluminescence emission threshold (*ca.* 1.2 atm) has been crossed. Above the incipient emission threshold, the light emission intensity is proportional to the drive-pressure amplitude (Bezzerides & Matula, unpublished data), until the extinction threshold is reached (*ca.* 1.4 atm), above which the bubble self-destructs.

(*a*) *Inertial cavitation threshold*

Between the region of linear spherical pulsations and nonlinear non-spherical unstable oscillations lies the inertial cavitation threshold. In figure 2 we plot the calculated steady-state radial motion of a 5 μm bubble in a 25 kHz sound-field, for various driving-pressure amplitudes. At low driving-pressure amplitudes, the bubble

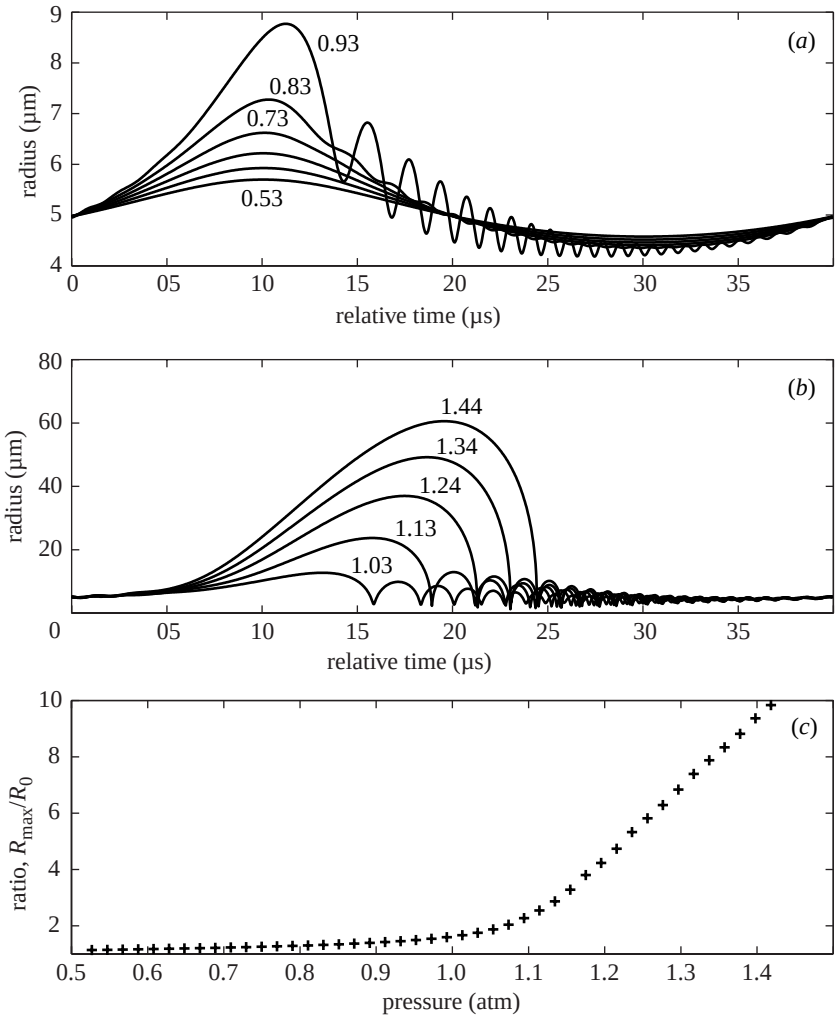

Figure 2. The steady-state oscillations of a 5 μm ambient size cavitation bubble in a 25 kHz sound field. In (*a*) and (*b*), the drive-pressure amplitude (in atmospheres) is given next to the actual curve, if space is available. In (*c*), the maximum radius is plotted as a function of the drive-pressure amplitude, normalized to the ambient radius. The inertial cavitation threshold is around 1 atm.

responds in phase with the sound field. As the drive amplitude is increased the bubble responds in a more nonlinear fashion. The difference in the growth of the bubble for various driving-pressure amplitudes can be easily seen by plotting the maximum radius attained during a given acoustic cycle (figure 2*c*). Note how the amplitude increases dramatically after about 1 atm for this set of parameters. This change in the rate of increase in the maximum radius of the bubble indicates a crossing of the inertial cavitation threshold. Experimental (uncalibrated) measurements of the linear and nonlinear pulsations of a bubble are shown in figure 3. Again note how the bubble becomes more nonlinear as the drive-pressure amplitude increases (from the bottom to the top of the plot).

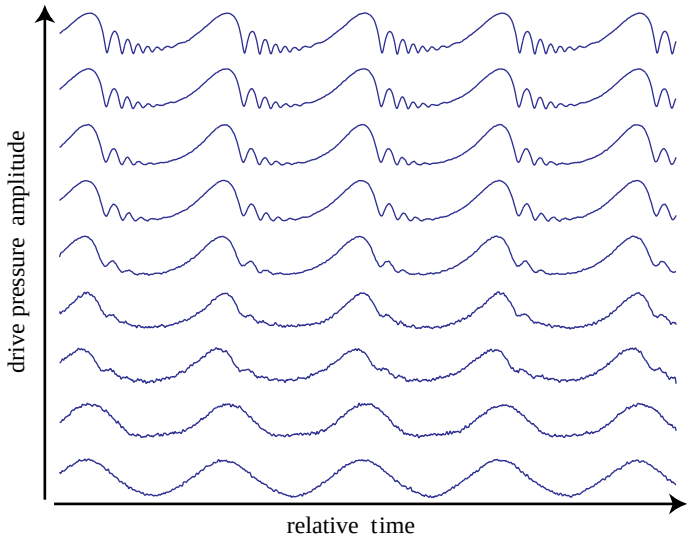

Figure 3. The measured uncalibrated radial oscillations of a cavitation bubble, as measured via light scattering. The data correspond to the square root of the light-scattered intensity. As the drive pressure is increased, the bubble develops a nonlinear shape, with afterbounces following the main collapse. The gas concentration used for this series of data was too high for stable SBSL. At the lower drive pressures, the bubble slowly dissolves. At the higher drive pressures, the bubble grows by rectified diffusion until it becomes unstable.

(*b*) *Stability regions*

Figure 4 illustrates the various regions in the drive-pressure parameter space, in this case, as a function of the ambient bubble size (for air bubbles at a given gas concentration) (Holt & Gaitan 1996). The region labelled 'd' corresponds to the dissolution region, where bubbles dissolve due to the excess surface tension (this region is analogous to the lowest region in figure 1). If the drive-pressure amplitude is increased further, the bubbles will grow by rectified diffusion; this region is labelled 'g'. The line separating the dissolution and rectified diffusion regions is called the rectified diffusion threshold. For a bubble driven at a particular pressure amplitude in region 'g', the bubble will grow towards the right until it reaches the boundary shown with data points. These points correspond to observed non-spherical oscillations (analogous to the 'dancing region' in figure 1).

Intuitively, one might expect that as the drive-pressure amplitude is increased further, the instabilities would simply grow, but, as alluded to in figure 1, there exist regions for bubble stability at higher pressure amplitudes, corresponding to stable SBSL. For the experimental conditions used in figure 4, stable SBSL occurs along the uppermost line (dark square data points), between about 1.3 and 1.4 atm. These researchers also found a stable, but non-sonoluminescent, stability line around 1.25 atm, shown as the lower dark square data points. Parenthetically, it is worth noting that there is a hysteresis effect; the drive-pressure amplitude for the incipient luminescence threshold is lower if approached from above the threshold, rather than approaching from below the threshold. Also, the extinction threshold apparently depends on the *rate* at which the threshold is approached (from below only, since the bubble cannot exist above the extinction threshold (Cordry 1995)).

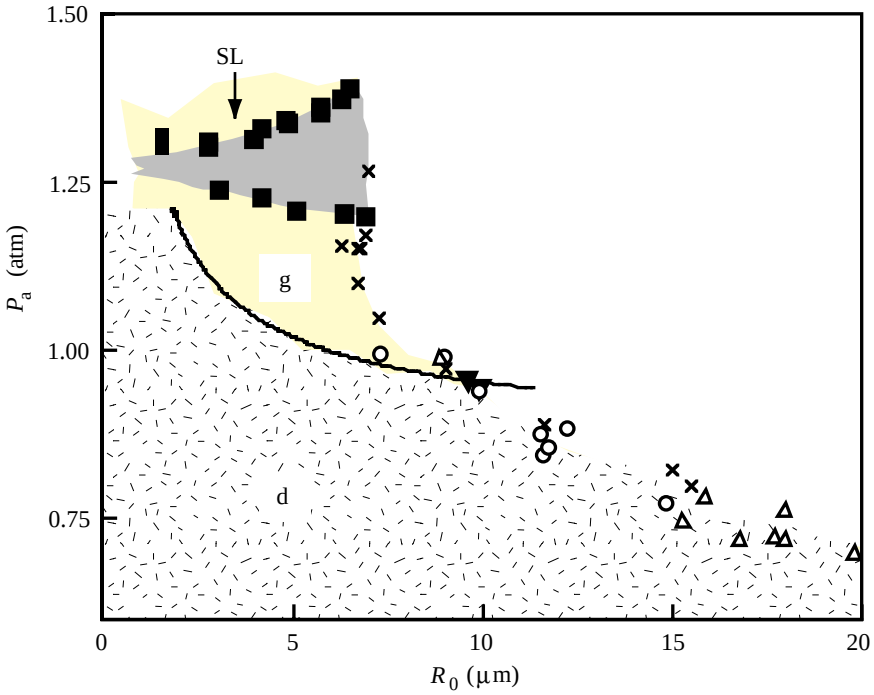

Figure 4. Instability thresholds for cavitation bubbles (compare with figure 1). Bubbles in the regions labelled 'd' dissolve, while those in the region labelled 'g' grow by rectified diffusion. The line separating these regions is the rectified diffusion threshold. The data points (labelled ○, × and △) at the edges of these regions are where the bubbles become spherically unstable. The different data points correspond to different instabilities. Sonoluminescence bubbles are shown along a line at the top of an 'island of dissolution'. (Courtesy of Holt & Gaitan (1996).)

The stability of SBSL is apparently governed by an equilibrium mass flux; over the course of a given acoustic cycle, there should be no net mass flux into or out of a stable bubble (the bubble should be in diffusional stability). Early attempts to model this behaviour resulted in large differences in the predicted versus observed gas content within the fluid. Figure 4, for example, shows the rectified diffusion threshold curve, which meets the 'no-net mass flux' criteria. This curve is far from the observed SBSL region. Recently, a new hypothesis has emerged to explain the apparent discrepancy between the modelled rectification curve and observed data. The hypothesis is based on the assumption that chemical reactions occur when the bubble is heated during its collapse (Lohse *et al*. 1997). For an air bubble, the species subject to chemical reactivity include N_2 and O_2. During the bubble collapse, the contents presumably heat up, dissociation occurs and new products are formed, such as NO_x compounds. According to the hypothesis, these product species irreversibly migrate into the fluid, leaving only the non-reactive species argon within the bubble interior. Thus, the initial air bubble quickly transforms into (mostly) an argon bubble. Under these conditions, one needs only to consider the partial pressure of argon, and not the concentration of air dissolved in the liquid.

Circumstantial evidence for this 'microreactor' hypothesis is found by noting that if one only considers the partial pressure of argon, the diffusional stability curve

Figure 5. Stable SBSL is generally accomplished in laboratory levitation cells, but can be generated in many different geometries. The author has generated SBSL in Coke^{TM} glasses, wine glasses, and other 'interesting' containers. Here, the glowing bubble is located near the centre of the glass.

matches the experimental data (Lohse 1997; Ketterling & Apfel 1998). Other experimental evidence supports this hypothesis as well (Matula & Crum 1998). Thus, one not only needs to consider mass flux, but also chemical activity, in order to satisfactorily explain the conditions found in light-emitting bubbles (we note that the conditions for sonoluminescence from cavitation fields, MBSL, are not equivalent to those in SBSL, since MBSL bubbles are not stable, cycle-to-cycle, but exist only transiently).

3. Experimental considerations

Typical experimental vessels for studying SBSL include spherical or round-bottom flasks, cylindrical tubes and rectangular or square-cross-section tubes. Each 'cell' has its own advantages and disadvantages. The spherical cell is symmetrically pleasing

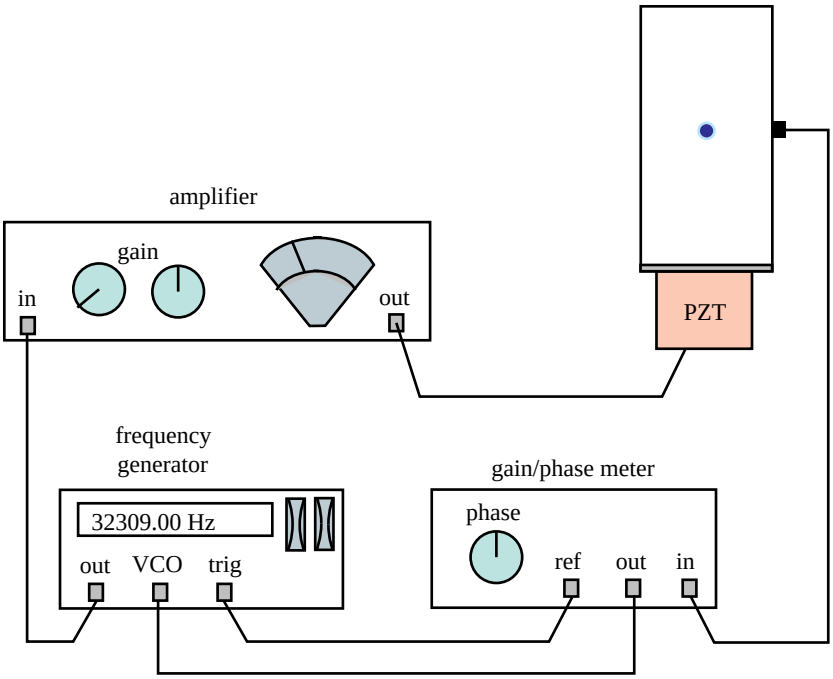

Figure 6. Transducers mounted to a cell in a variety of configurations can be used to set up a standing wave field. A side pill transducer is used to monitor the phase of the pressure field relative to the function generator output. The phase meter and voltage controlled oscillator (VCO) of the function generator can be used to maintain the system's resonance.

and easy to close off from the surrounding atmosphere; however, the curvature may present problems with transducer mounting, aligning and refraction of light; a similar problem exists with cylindrical cells. Rectangular-cross-section cells are simple to work with in most cases, especially if trying to image the bubble. Note that non-symmetric geometrical cells do not preclude bubble levitation and SBSL. Figure 5 shows a stable glowing bubble in a dinner glass. The importance of a quality three-dimensional standing wave cannot be over-stated, however.

The fluid used in most studies of SBSL is filtered degassed water. In the simplest case, tap water can be degassed by boiling for approximately 15 min, and then cooled in a closed container before the experiment begins. Aspirators are also useful for quick degassing. These approaches work well if the gas concentration is not an important parameter that is being controlled. For more precise studies, a closed system that incorporates gas-pressure and system-temperature monitoring is more appropriate; gas ports are used to introduce specific concentrations and types of gas, while fluid ports allow fluid transfer without contamination or introduction of atmospheric gases.

A transducer mounted directly to the outside of the cell can be used to generate a standing pressure wave within the cell. Typical transducers include hollow cylinder and disk piezoceramics (PZT). The PZT is driven by a power amplifier, which in turn is supplied with an appropriate sinusoidal signal, at a frequency corresponding to a normal mode of the cell, from a function generator (figure 6 illustrates the set-up).

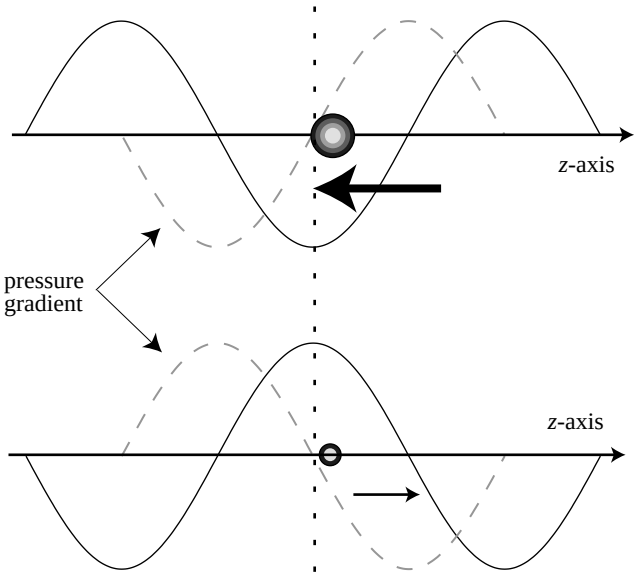

Figure 7. Levitation of a small bubble at a pressure antinode. When the bubble is large (during the tensile phase of the sound field) the force is directed towards the antinode. When the bubble is small (during the compressive phase of the sound field), the force is directed away from the antinode.

(*a*) *Bubble levitation*

Physically, the acoustic radiation force required to levitate a bubble in a standing wave field arises from a pressure difference (gradient) across the bubble (Eller 1968). The force on the bubble is time dependent, and varies according to the phase of the sinusoidal pressure field. Figure 7 illustrates this force for the case of *small* driving pressures (and for drive frequencies below the bubble's natural resonance frequency; see Matula *et al.* (1997*a*, *b*)). During the negative portion of the sound field the bubble grows. There is a pressure force on the bubble due to a slight difference in pressure exerted on either side of the bubble's surface. This force directs the bubble towards the pressure antinode. During the compressive phase of the sound field the bubble is small and the force is directed away from the pressure antinode; however, since the corresponding volume is smaller, this force is smaller, and hence, over an acoustic cycle, the average radiation (or Bjerknes) force directs the bubble towards the antinode. (This argument on the direction of the force applies only to a bubble that is driven below its natural resonance frequency. For bubbles driven above their natural resonance frequency, a different phase response requires them to be forced away from the pressure antinode and toward a node.)

Though valid at lower drive-pressure amplitudes, this description of the Bjerknes force must be modified at higher driving pressures. Under moderately large pressure amplitudes, the bubble may continue to expand after the pressure turns positive, before finally undergoing a violent inertially dominated collapse. As the drive-pressure amplitude increases, the phase (time) of collapse continues to increase. Pedagogically, one can envision that as the drive pressure is increased further and further, the phase of collapse will continue to increase until the next acoustic cycle interferes with the bubble's motion. What actually occurs is somewhat more subtle.

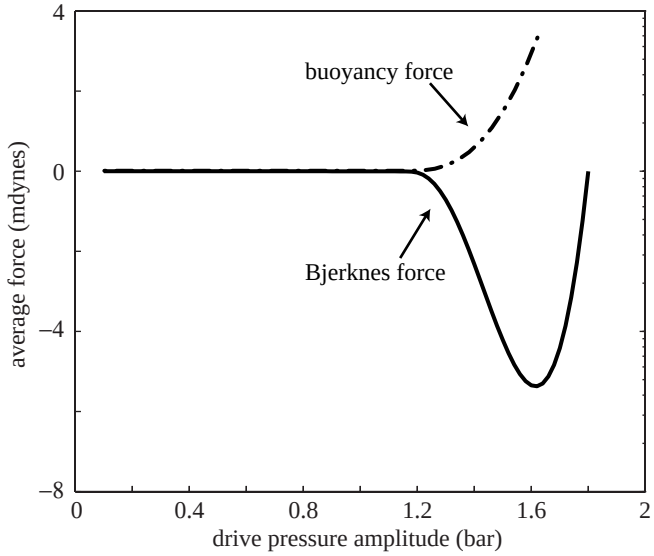

Figure 8. The Bjerknes and buoyancy forces on a small bubble (from equation (3.1)). These calculations assume that the size of the bubble does not change as the drive-pressure amplitude is increased. Although this assumption is not valid, there is only a slight dependence on bubble size over the region occupied by SBSL.

Consider that the average acoustic radiation force must balance the average buoyancy force in order to levitate a bubble. This relation can be expressed as

$$\frac{\rho g}{T}\int_0^T V(t)\,\mathrm{d}t = \frac{k_z P_\mathrm{a}}{T}\sin(k_z z)\int_0^T V(t)\sin(\omega t)\,\mathrm{d}t, \tag{3.1}$$

where ρ is the fluid density, g is the acceleration due to gravity, $V(t) = \frac{4}{3}\pi R^3(t)$ is the bubble volume, $k_z = 2\pi/\lambda_z$ is the vertical wave number, T is the acoustic period, z is the average equilibrium position of the bubble above the pressure antinode (where $z = 0$), and P_a is the applied drive-pressure amplitude. Note that the bubble is assumed to be spherical, and the acoustic radiation force is parallel to the gravitational force. With no body forces in the horizontal plane, the symmetry of the sound field should preclude a horizontal component of the acoustic radiation force.

Figure 8 plots the average acoustic radiation, or Bjerknes force (the right-hand side of equation (3.1)), as well as the average buoyancy force (the left-hand side of equation (3.1)) using experimental parameters (Matula *et al*. 1997*a*). Note that the Bjerknes force is negative for drive-pressure amplitudes below about 1.8 atm. Above this value, the average force actually pushes the bubble *away* from the pressure antinode, thus precluding bubble levitation at these high drive-pressure amplitudes.

From equation (3.1), a simple expression for the average equilibrium levitation position of the bubble can be obtained, provided one assumes the bubble is located near the pressure antinode. Then $\sin(k_z z) \approx k_z z$, and

$$z \approx \frac{\rho g}{k_z^2 P_\mathrm{a}}\frac{\Lambda_1}{\Lambda_2}, \tag{3.2}$$

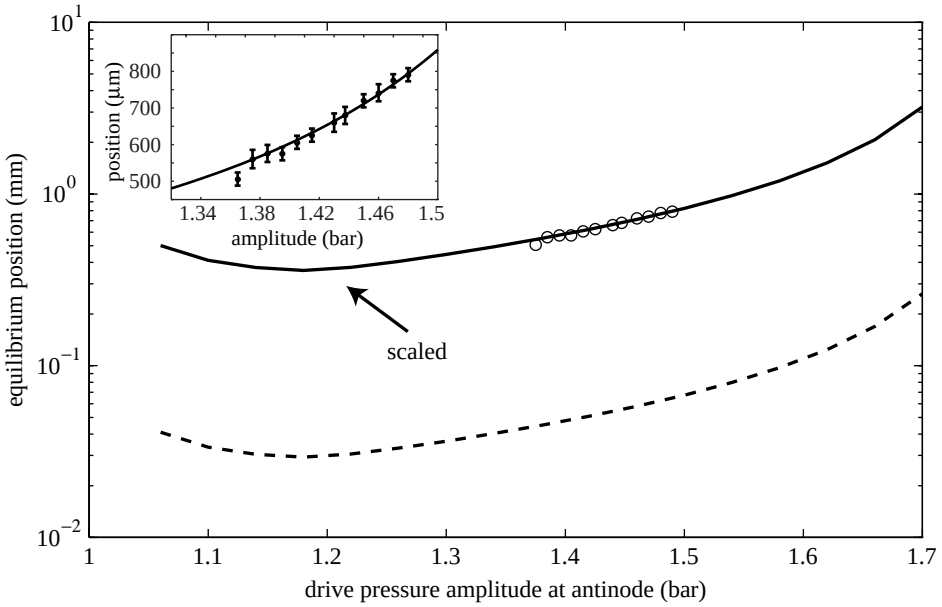

Figure 9. The equilibrium bubble levitation position, as a function of drive-pressure amplitude. For small drive pressures (not shown here), the bubble position is inversely proportional to the drive-pressure amplitude. At higher drive pressures, the bubble is levitated further from the antinode. The calculation is in qualitative agreement with the data in the sonoluminescence regime (shown as circles), but differs quantitatively by a scaling factor.

where

$$\Lambda_1 = \int V(t)\,\mathrm{d}t \quad \text{and} \quad \Lambda_2 = \int V(t)\sin(\omega t)\,\mathrm{d}t,$$

from equation (3.1).

Figure 9 plots the average equilibrium bubble position from equation (3.2) (dashed line) above the antinode as a function of the applied pressure amplitude (for a 5 μm bubble driven at 19.5 kHz). From equation (3.2), for small drive pressures the equilibrium position of the bubble is inversely related to the drive pressure, in agreement with linear theory. However, as the drive pressure is increased further, the bubble's equilibrium position begins to shift *away* from the antinode (figure 8, which shows that as the pressure increases, the Bjerknes force on the bubble becomes smaller in magnitude). Note that as the drive-pressure amplitude increases, the average equilibrium location of the bubble is further from the pressure antinode, and thus the bubble 'feels' a slightly smaller pressure amplitude than the maximum value at the pressure antinode. However, this apparent decrease in pressure felt by the bubble is offset by the increase in the drive-pressure amplitude, at least in our approximation.

Also shown in the figure are experimental measurements of the average equilibrium position of a sonoluminescing bubble, determined by using a microscope. Note that the qualitative features of the calculation agree well with experiment, however, there appears to be a large scaling discrepancy. The mechanism for the observed discrepancy may involve the interaction of the bubble with the sound field. Consider that with the bubble present, the measured vertical pressure profile flattens out considerably near the bubble (Matula *et al.* 1997*a*). We can fit this flattened profile

near the bubble by assuming a wavelength 3.5 times the original wavelength. If this pressure flattening is real (and not simply due to scattering from the bubble), then we recover the scaling factor that we needed for quantitative agreement with measurements. The observed discrepancy may also be due to experimental conditions; the quality of the resonance may affect the bubble's position and stability significantly. (Note that previous studies of bubble levitation in a stationary wave have been carried out for bubbles larger than resonance size, where the bubble is levitated near a pressure node (Asaki & Marston 1994, 1995), and for bubbles smaller than resonance size (Crum & Eller 1970; Crum & Prosperetti 1983), in both instances, driven into small-amplitude oscillations. Our results are for bubbles below resonance size, driven into highly nonlinear spherical pulsations.)

It is interesting to note that in the absence of gravity there is no buoyancy force, and thus it may be possible to levitate a bubble almost exactly at the pressure antinode, instead of slightly above the antinode. Under such conditions, one may be able to drive the bubble to a much larger volume expansion, and achieve greater light output during the collapse. Of course, this assumes that observed surface instabilities do not limit the collapse energy. If these observed instabilities are due to the translational motion of the bubble (due to periodic variations in the buoyancy and acoustic radiation forces), then increasing the energetical collapse of SBSL bubbles should be achievable in a microgravity environment. There is some preliminary evidence that this is indeed the case (Matula *et al.* 1996*b*, 1997*a*, *b*), although more studies need to be undertaken to verify that gravity plays a role in defining the stability regions in SBSL.

(*b*) *Hydrophone measurements of the driving acoustic pressure amplitude*

One of the most important parameters associated with sonoluminescence is knowledge of the driving acoustic pressure amplitude. Measuring the pressure amplitude is difficult since hydrophones that are small enough to minimally disturb the pressure profile are typically only calibrated at high frequencies (above 1 MHz). Our method for calibrating small-needle hydrophones is described here. The technique involves levitating bubbles at *low* acoustic pressure amplitudes, and measuring their size and displacement from the pressure antinode (Gould 1967).

Starting with equation (3.1) and a bubble-dynamics equation (such as the Rayleigh–Plesset equation), and linearizing the bubble radius, one can write the drive-pressure amplitude as (Eller 1968)

$$P_{\mathrm{a}}^2 = \frac{2\rho g \lambda \kappa P_0}{\pi \sin(4\pi z/\lambda)} \left[\frac{4\pi^2 f^2 \rho R_0^2}{3\kappa P_0} - 1 \right], \tag{3.3}$$

where ρ is the liquid density, g is the acceleration due to gravity, λ is the *vertical* wavelength of the acoustic levitation field, κ (here taken as unity) is the polytropic exponent, P_0 is the ambient pressure, f is the drive frequency, R_0 is the ambient or equilibrium radius, and z is the equilibrium distance above the pressure antinode.

The known quantities in equation (3.3) include the driving frequency, ambient pressure (which should always be measured by using a barometer), and the density. The *vertical* wavelength, ambient radius and bubble position above the antinode must be measured in order to determine P_{a} (at low driving pressures, to ensure the validity of equation (3.3)). Using the small-needle hydrophone, one can map out the

pressure profile in the cell and thus determine both the wavelength, and the location of the antinode (where $z = 0$). The size and location of the bubble can be determined by using an imaging technique (described below), thus giving the pressure amplitude necessary for levitating a bubble at a particular position above the antinode. Care must be taken when imaging the bubble size, since the bubble is actually oscillating. If the size of the bubble is measured at two points in the acoustic cycle, separated by 180°, the average of those two measurements will give the ambient radius (assuming low driving pressures that result in linear oscillations of the bubble).

It's important to note that a constant voltage output into the transducer used to generate a standing pressure wave does not necessarily imply that the driving-pressure amplitude is constant. Changes in temperature, etc., can result in a detuning of the levitation cell, resulting in a shift of the response curve, and a change in the drive-pressure amplitude. Changes in the response of the system can be monitored by measuring the phase of the sound field with respect to the signal generator, as illustrated in figure 6 (Hiller 1995).

4. Bubble-dynamics measurements

This section describes techniques for monitoring a bubble's dynamic motion, (or 'radius–time' or $R(t)$ curve). Methods for observing the dynamic motion of the bubble include light scattering and direct imaging. Measurements of the *properties* of the emitted light and sound from the bubble are described in the next section.

(*a*) *Light scattering*

Assuming that the bubble remains spherical, direct light scattering off the bubble can be used to record the $R(t)$ curve, as shown in figure 3. Figure 10 illustrates the basic set-up used to record the dynamical response of the bubble, together with a measured signal over one acoustic cycle. Experimentally, a 10 or 30 mW HeNe laser is sufficient to record the $R(t)$ cycles. A large lens placed near the cell is then used to focus the scattered light onto the photodetector, typically a photomultiplier tube (PMT). Unfortunately, the dynamic range of the PMT is not sufficient to observe in high quality both the maximum size and rebounds, or afterbounces, of the bubble's motion. If both regions are to be studied, an acousto-optic modulator (AOM) can be used to regulate the incident intensity of the laser light. Also, the finite bandwidth of the PMT will limit the resolution of the collapse so that probing the bubble near its minimum radius requires a fast photodetector, such as a streak camera.

Although the general theory that describes light scattering from bubbles can be complicated, it simplifies considerably over most of the region of interest for sonoluminescence bubbles. Under these appropriate conditions, the intensity of the scattered light is proportional to the square of the bubble radius. Thus, by measuring the size of the bubble, say at its maximum radius, one can then determine the bubble size for the rest of the cycle. Bubble dynamics codes show a good fit with experimental data, as shown in figure 10; however, the full Mie theory must be used for probing the bubble's size near its minimum radius.

(*b*) *Imaging*

In order to determine the calibration constant for the $R(t)$ curve, described above, the bubble's size must be measured at some point in the cycle. Using a microscope,

PHILOSOPHICAL TRANSACTIONS OF THE ROYAL SOCIETY A MATHEMATICAL, PHYSICAL & ENGINEERING SCIENCES

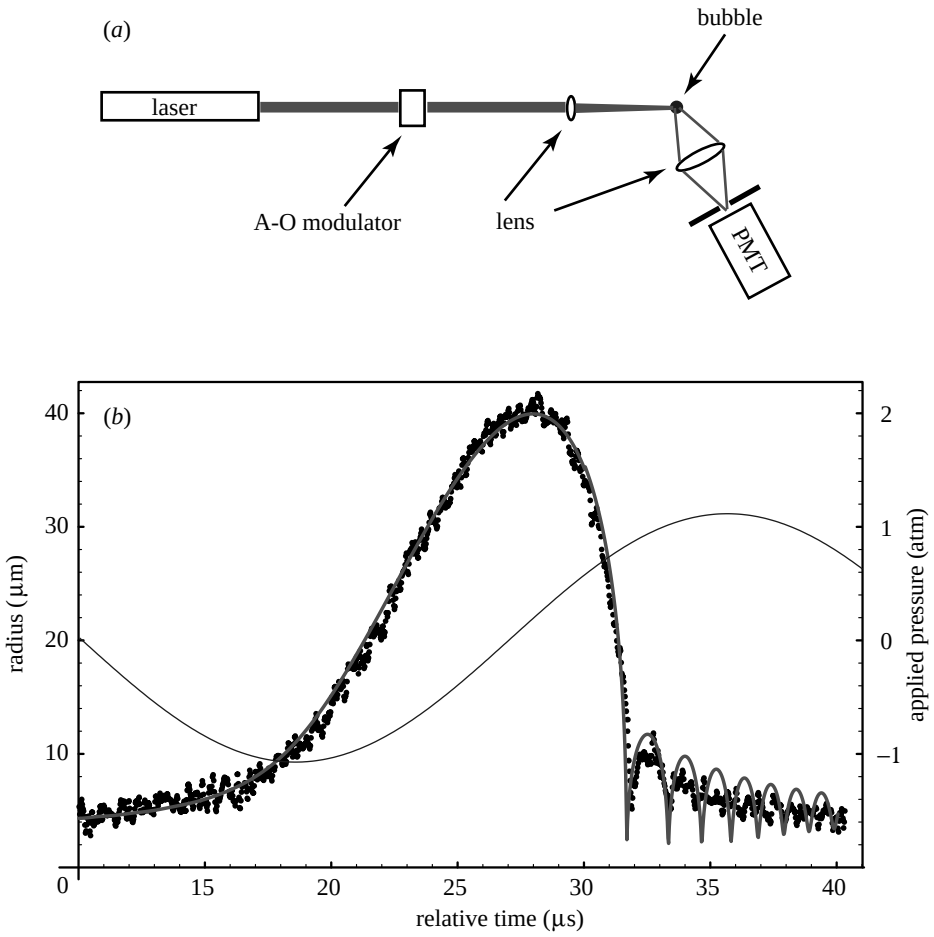

Figure 10. (*a*) Light-scattering technique for measuring the radial oscillations of a sonoluminescence bubble. (*b*) Instantaneous scattered intensity collected from a pulsating bubble. In the geometrical optics limit, the scattered intensity is proportional to the square of the bubble radius. The normalized drive pressure is shown as well. The data (non-averaged) fit nicely with the Keller–Miksis nonlinear bubble-dynamics equation. Figure 3 was also obtained with light scattering.

fast LED and CCD camera, it is simple enough to measure the maximum bubble size (see figure 11). This calibration point can then be used to determine $R(t)$ over most of the acoustic cycle.

It is also possible to use the imaging set-up to measure the $R(t)$ curve directly (Tian *et al*. 1996). If the phase of the LED flash is continuously changed, the $R(t)$ curve can be mapped out. The advantage here is that the radius is measured directly. Furthermore, the important information that is required is usually the ambient, or equilibrium, radius and the maximum radius. These two points can be obtained quickly with the imaging system. The disadvantages include not being able to measure the radius over a given acoustic cycle (the bubble must be stable, cycle-to-cycle), and the large errors in measuring the bubble's size below about 5 μm. Note that the

imaging system must also be calibrated, for instance by imaging a grooved calibration slide.

(c) *Non-sinusoidal excitation*

Most studies with sonoluminescence involve a sinusoidal drive; however, non-sinusoidal excitation of a cavitation bubble is not precluded. Researchers found that the addition of a second harmonic to the fundamental drive frequency resulted in an increase in the emission intensity from SBSL above the maximum attainable intensity from a single frequency drive (Holzfuss 1998). Here we examine the bubble dynamics of a sonoluminescence bubble with harmonic excitation. Figure 12 shows various $R(t)$ curves obtained by adding a third harmonic at various phases relative to the fundamental. In most cases, we are able to fit the experimental curves with a bubble-dynamics equation (the Keller–Miksis equation), using only the ambient radius of the bubble as a fitting parameter. In some cases, the harmonic excitation results in the bubble being displaced from the central region of the levitation cell, and thus we believe that our pressure measurements are not reliable in those cases, precluding a good fit to the bubble-dynamics equation.

(d) *Non-spherical bubbles*

The light-scattering system described above can also be used to record instabilities in the radial motion of a cavitation bubble. Figure 13 shows the instantaneous cycle-to-cycle light-scattered signal of the rebounds or afterbounces from a bubble in the 'dancing' region of the drive-amplitude parameter space. Notice the spikes in the light-scattered signal near $t = 8.5$, 10.5 and 11.5 ms. These spikes may be caused by light-focusing from the non-spherical bubble, and probably indicate a parametric instability (images of the bubble showed non-spherical oscillations). These spikes are usually not observed in stable SBSL. Note that Mie scattering theory cannot be used under these circumstances to relate the scattered light intensity to a bubble size, since the theory only applies to spherical objects.

5. Acoustic and electromagnetic emissions from SBSL

The time scales that are involved with SBSL cover many orders of magnitude. The duration of the sonoluminescence light flash (as well as the jitter in the bubble's stability) is measured in picoseconds (Barber & Putterman 1991; Gompf *et al*. 1997; Hiller *et al*. 1998); the duration of the acoustic emission from a sonoluminescence bubble has been measured in nanoseconds (Gompf *et al*. 1998*a*, *b*; Matula *et al*. 1998); the period of the sound field used to drive the bubble into oscillations is measured in microseconds; the lifetime of the bubble can last milliseconds, seconds, minutes or even hours, depending on the fluid and gas content and external influences; thus, many measurement techniques are used. Some of these measurements are described here.

(a) *Acoustic emissions from SBSL*

If a small hydrophone is placed near a pulsating bubble, large signals can be observed. These signals correspond to the acoustic emission from the cavitating bubble. Figure 14*a* shows the temporal history of an acoustic signal emanating from

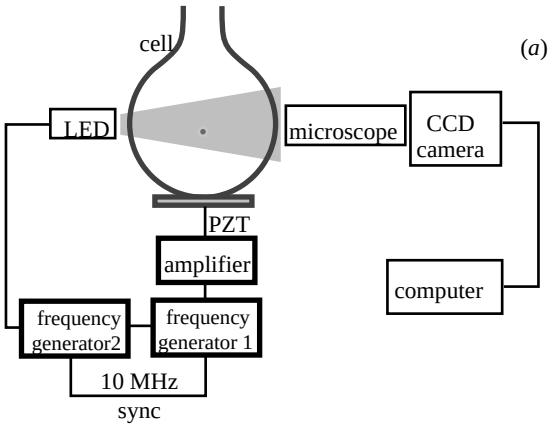

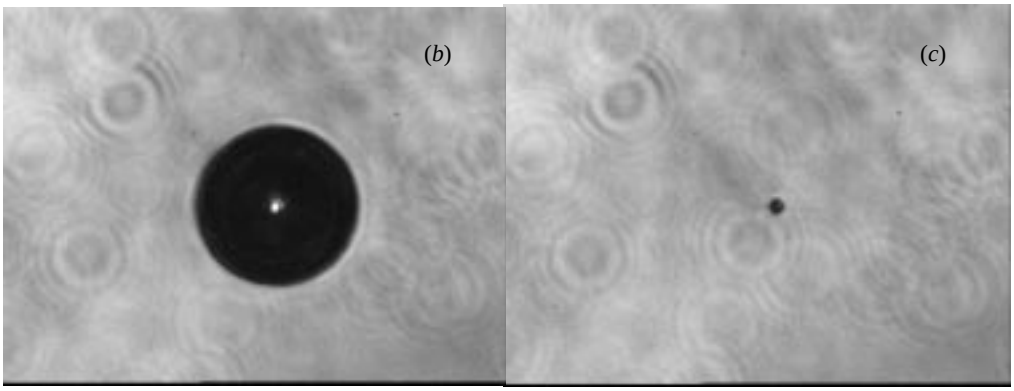

Figure 11. (*a*) Imaging technique to measure the radial oscillations of a sonoluminescence bubble. Backlighting produces a shadow image of the bubble. With a spherical cell, as shown here, a flat window is cemented to a cut-out portion of the cell in order to image the bubble clearly. A rectangular cell can be used as well. (*b*) An image of the bubble near its maximum size of about 60 µm. The bright spot at the centre of the bubble image is probably due to direct passage of the light through the bubble. (*c*) An image of the bubble at its ambient size, about 6 µm. Note that the CCD shutter is open over a relatively long time, but the LED is strobed in a synchronous fashion, and thus the bubble is illuminated for only about 200 ns each acoustic cycle. The bubble must remain stable for many cycles in order to obtain clear images.

a sonoluminescence bubble (an acoustic emission can also be measured below the luminescence threshold; see Matula *et al.* (1998)). For this case, a high-frequency calibrated 250 µm element-size hydrophone was placed approximately 1 mm from the bubble. Note the relatively large pressure amplitude (*ca.* 1.7 atm), even at this distance. Assuming only spherical spreading causes attenuation of the acoustic pulse, the amplitude of the pulse at 1 µm would be approximately 1700 atm. More recent measurements indicate that the emitted shock wave near the bubble is much higher (Gompf 1998*b*).

Similar measurements of the acoustic emission can be made by using a focused transducer, acting as a receiver. In this case, the transducer is positioned so that the bubble location is at the focus of the transducer. The focusing gain of this transducer

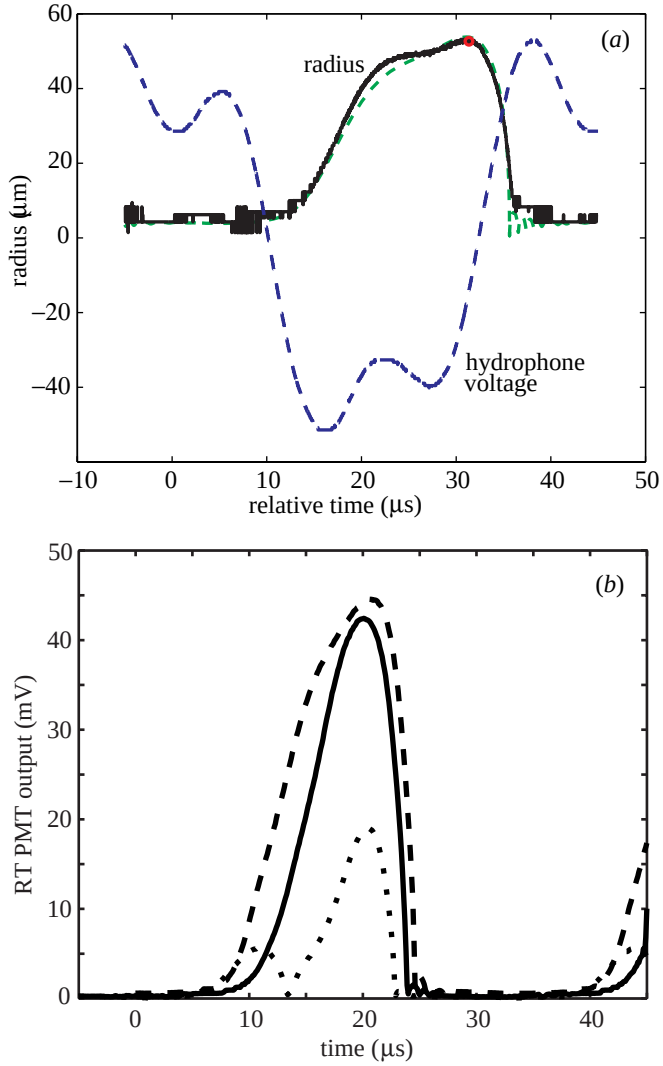

Figure 12. Harmonic excitation of SBSL. In (*a*), the third harmonic is added to the fundamental drive frequency to produce a broadened $R(t)$ curve. The pressure profile is shown as a dashed line. The equilibrium radius was measured to be 5.1 μm by using a microscope, and a best fit to the Keller–Miksis equation generated an equilibrium radius, $R_0 = 4.9$ μm. The fundamental pressure amplitude was measured to be $P_f = 1.37$ atm, while the third harmonic was measured at $P_3 = 0.49$ atm. The phase difference (out of the function generator) was $\Delta\vartheta = 171.8°$. In (*b*), it is shown how the $R(t)$ curve can change by varying the phase between the fundamental and the third harmonic (the solid line corresponds to no third harmonic added). In all three cases, the bubble was stable and emitting light.

is sufficient to even allow observations of the acoustic emissions of the afterbounces (figure 14*b*). Using a pulse–echo technique to locate the position of the bubble, and simultaneous light scattering, the acoustic emission is found to coincide with the minima of the bubble collapse. The acoustic pulses are probably due to the bubble arresting its inward collapse. That is, as the bubble collapses to a minimum value, it

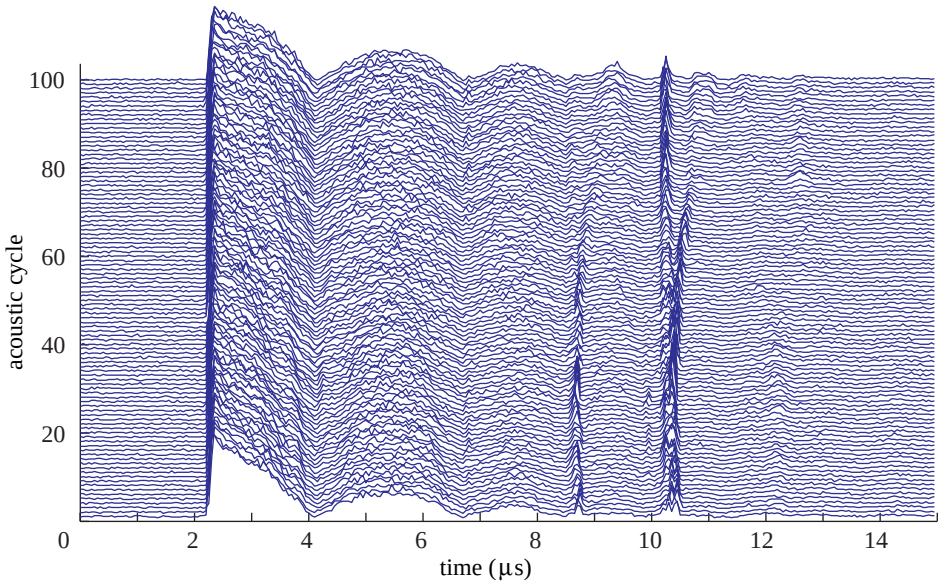

Figure 13. The afterbounces of a bubble driven below the luminescence threshold. Parametric instabilities can be inferred from the light-scattered signal. Note the large signal spikes near 9 and 10.5 μs in this figure. Direct imaging of the bubble shows non-spherical bubble shapes.

must decelerate. This *inward* deceleration corresponds to an *outward* acceleration, which results in an emitted pressure pulse.

(*b*) *Photomultiplier measurements of the light emission, and constraints*

The light emission from sonoluminescence is usually too dim to observe with photodiodes; thus, the photomultiplier tube (PMT) is an invaluable tool for making the necessary measurements. A PMT is also used for light-scattering $R(t)$-curve experiments, and for collecting spectra. It is beyond the scope of this paper to discuss all the parameters that influence the PMT measurement. Some important parameters that need to be recognized include: the wavelength window (wavelength region over which the PMT is sensitive to incident photons); the quantum efficiency (a measure of the efficiency of the PMT to convert a photon into an electron and have it observed at the anode); the rise-time of the signal; the transit-time spread (TTS); and gain. A brief description is included here; details are available in Engstrom (1980).

1. *Wavelength sensitivity.* Owing to the photocathode material and the cover window, the sensitivity of a PMT usually ranges from about 200 to 800 nm, with a peak sensitivity at around 440 nm. Specialized detectors are available for observing regions outside this range.

2. *Quantum efficiency.* The quantum efficiency of a PMT refers to the probability of generating a signal at the anode, given an input of a photon. The probability of a photon dislodging an electron (a photoelectron) and generating a signal at the anode is usually less than 30%, depending on the particular PMT. Assuming photoelectron conversion of incident photons is additive independent, the

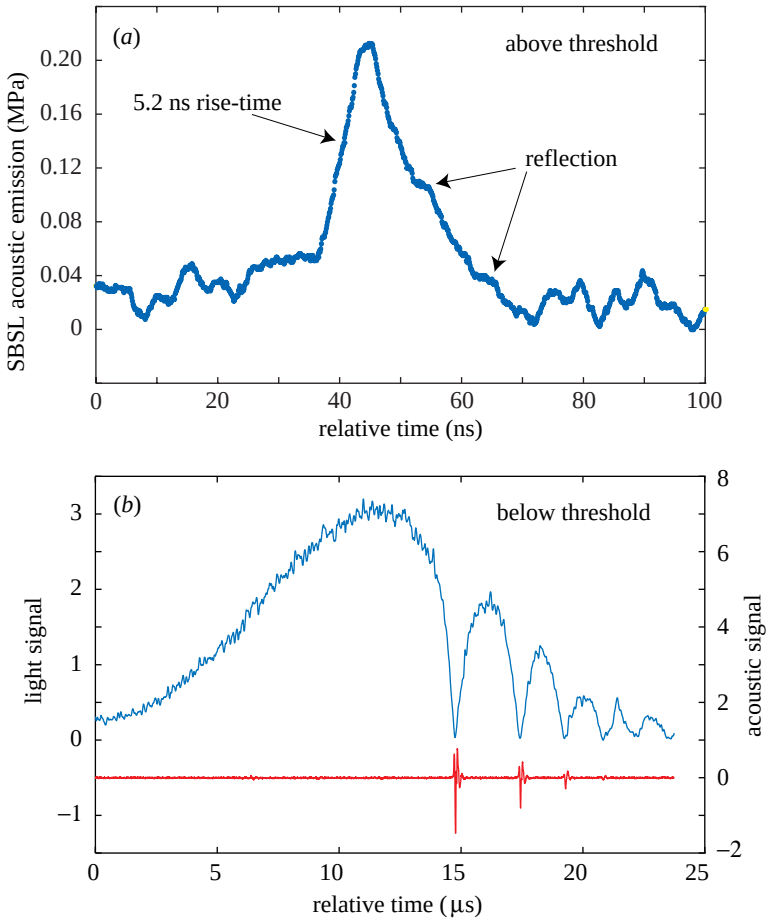

Figure 14. (*a*) The acoustic emission from a sonoluminescence bubble using a small (250 μm element size) PVDF needle hydrophone located 1 mm the bubble. The rise-time of the signal, *ca.* 5.2 ns, is, in part, limited by the finite bandwidth of our system and by the finite curvature of the wavefront. The regions labelled 'reflection' are due to the finite thickness of the PVDF hydrophone element. (*b*) Large acoustic signals can be observed if the bubble is placed at the focus of a transducer. Here we show simultaneous light scattering and acoustic detection with a focused transducer. The acoustic signal is translated in time corresponding to the time it takes sound to travel from the bubble to the transducer. In this way, we see that the acoustic signals originate from near the bubble minima. Acoustic emissions from the afterbounces can also be observed in this case. In (*b*), the bubble was driven below the luminescence threshold. Acoustic signals are observed both below and above the luminescence threshold.

probability for photoelectron emission (p) as a function of the number of incident photons (m) is

$$p_r(\varepsilon) = \varepsilon^r (1-\varepsilon)^{m-r} \frac{m!}{r!(m-r)!}. \tag{5.1}$$

Here, ε is the quantum efficiency of the PMT (e.g. 0.15 at 440 nm for one particular type of PMT), and r is the number of photoelectrons emitted from the photocathode. In words, the probability for photoemission of r electrons

is given by the probability for emission of all the electrons multiplied by the probability for no emission multiplied by the number of ways for combining the probabilities (the binomial distribution). For example, even for a 10-photon pulse incident on the photocathode described above, the probability that no photoelectrons are emitted from the photocathode is $p_0(0.15) = 0.20$. Thus, there is a 20% probability that no pulse is observed at the anode of the PMT when the photocathode is subject to an incident burst of 10 photons!

3. *Transit time spread (TTS).* The transit time refers to the time interval between the photon incident on the photocathode, and the corresponding signal at the anode. The spread in this time interval (TTS) is mainly due to the spread of velocities and directions of electrons emitted from the photocathode of the PMT, and may affect the rise-time of the pulse. For example, two identical photons emitted from a single source, and incident on two identical PMTs, will result in a slight difference in the arrival time of the pulse, and a slight difference in the pulse shape. The TTS puts limitations on the ability to detect very small time differences.

4. *Impulse response.* The response of a PMT from a single photoelectron corresponds to the impulse response of the PMT. Due to the PMT's quantum efficiency and TTS, the pulse width and shape can vary somewhat. Typically, the pulse shape approximates a Gaussian function. Thus the rise-time of the pulse is $\tau \approx 1.69\sigma$, where σ is the standard deviation of the Gaussian function. Similarly, the FWHM of a Gaussian is given by FWHM $\approx 2.36\sigma$, so that FWHM $\approx 1.4\tau$. Note that the finite rise-time of the signal must be taken into account when performing light-scattering measurements.

(*c*) *Pulse width measurements of SBSL*

Sonoluminescence flashes are too short to resolve by using PMTs, even high-speed multichannel plate PMTs. Two approaches are currently used to measure the pulse width of SBSL. One method uses a streak camera, in which it may be possible to measure the pulse width from a single SL flash. Current efforts are underway to increase the SBSL light intensity in order to increase the signal-to-noise ratio for this system.

A second (less-expensive) method uses time-correlated, single-photon counting (TC-SPC) (O'Connor & Phillips 1984). Figure 15*a* illustrates the set-up. Photons from the *same* SL flash pass through narrow bandpass filters (so that the photons have the same energy) and are incident on two opposing PMTs. The output from each PMT goes into a constant fraction discriminator (CFD), which outputs a precise timing signal. These timing signals are then collected by a time-to-amplitude converter (TAC), which outputs a DC voltage proportional to the time between the two inputs.

A histogram from the TAC gives not only the pulse width, but also the pulse shape. Such a system can resolve pulse widths from SBSL below 50 ps (depending on the resolution of the individual components). It is important that the bubble remains stable for this technique to work properly. Figure 15*b* shows an experimental pulse shape obtained by using this technique (Gompf *et al.* 1997). Note that there is an asymmetry in the pulse shape. Since the TC-SPC approach to measuring the

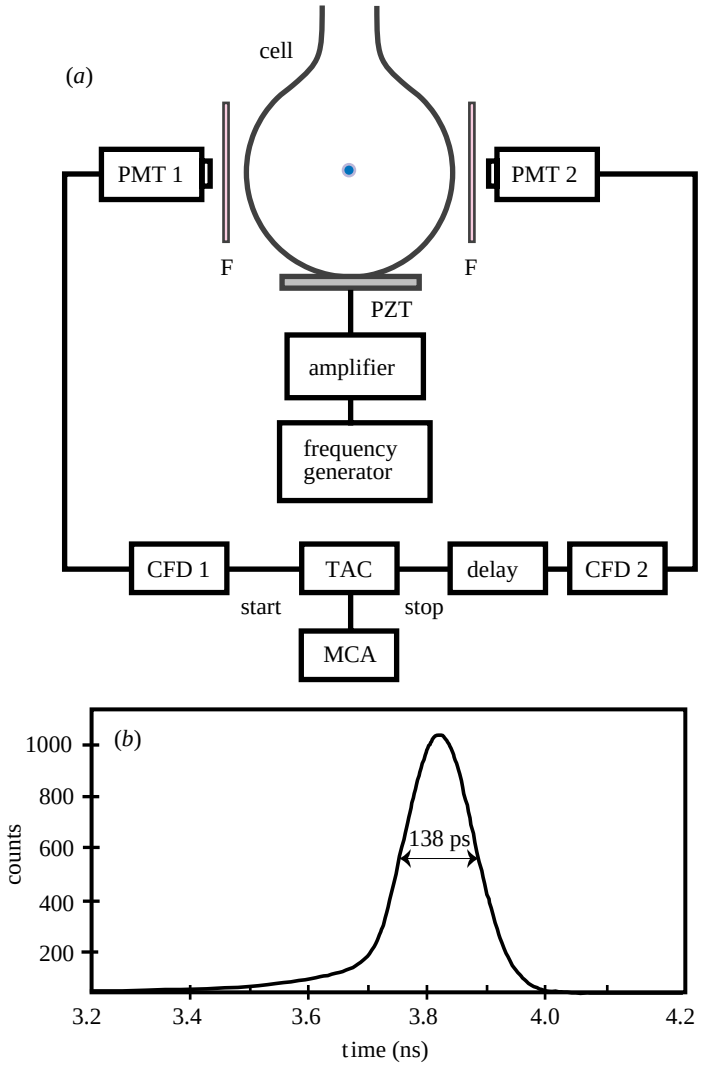

Figure 15. (*a*) Experimental set-up for measuring the duration of a sonoluminescence pulse. This method requires a stable bubble so that a histogram can be built up from many individual signals. (*b*) Pulse shape from SBSL using the technique in (*a*). Note that the pulse is somewhat asymmetrical. Recent data show that this asymmetry is actually reversed; the tail occurs *after* the main emission. (From Gompf *et al*. (1997).)

pulse width essentially involves an autocorrelation, the direction of the data set is arbitrary. Recent results with streak cameras have shown that the tail in the pulse shape occurs after the main pulse, and not before, as shown in this figure. Thus, there is an 'afterglow' associated with SBSL (Gompf *et al*. 1998*a*).

6. Single-bubble versus multibubble sonoluminescence

MBSL refers to sonoluminescence from a field of cavitating bubbles. These bubbles are influenced not only by the large acoustic pressure amplitudes, but also by other

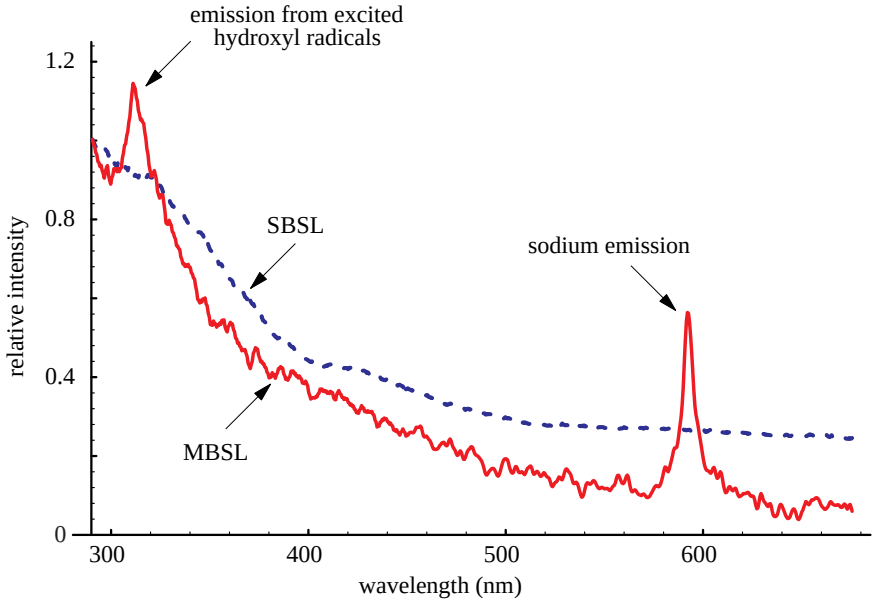

Figure 16. Comparison of the background subtracted spectra of MBSL and SBSL in a 0.1 M NaCl solution. Each spectrum was normalized to 290 nm. Absolute radiance comparisons cannot be made due to differences in light-gathering techniques. Note the prominence (in MBSL) and absence (in SBSL) of the sodium emission line near 589 nm. The peak in the MBSL spectrum near 310 nm is indicative of recombination of excited hydroxyl radicals.

nearby bubbles, as well as by the vessel walls. It is probable that bubbles in a cavitation field cannot survive more than a few acoustic cycles before breaking into smaller microbubbles, and, thus, probably do not show evidence for gas exchange, as discussed in a previous section. Nevertheless, some useful comparisons can be made. For instance, if one examines the pulse duration from MBSL by using fast optics and digitizers, the duration (or pulse width) is found to be less than about 1 ns (Matula *et al*. 1996*a*), which is similar to the pulse duration of SBSL.

(*a*) *Spectral comparisons*

Another area of comparison between MBSL and SBSL that has recently been explored is the spectral characteristics of the light emission. In a study comparing the spectral characteristics from an aqueous solution containing sodium chloride, it was found that the sodium doublet, which is prominent in MBSL, is completely absent in SBSL (see figure 16 and Matula *et al*. (1995)). One possible explanation for this difference is in the dynamics of the bubble(s). SBSL bubbles appear to be spherical through most of the acoustic cycle. There is no mechanism for sodium, which is non-volatile, to enter the bubble's interior, where it can be heated to incandescence. MBSL bubbles, on the other hand, are subject to intense pressures and pressure gradients that result in non-spherical pulsations; thus, there are several mechanisms for sodium to become entrained within these bubbles, resulting in a sodium emission upon heating of the bubble interior.

Although there are differences in the spectra, note that there is a similarity in the underlying continuum. This similarity may be interpreted by assuming some MBSL

bubbles act like SBSL bubbles, giving rise to the continuum, while other bubbles are much cooler and give rise to line and band emissions. Previous interpretations have described the continuum as a series of overlapping band emissions, with some experimental evidence to support that hypothesis (Seghal *et al*. 1980); however, recent experiments have cast some doubt on the older experimental results (McNamara *et al*., unpublished data). In any case, it is apparent that the commonality of cause (acoustic cavitation) and effect (light emission) for both types of sonoluminescence suggests some association of the underlying physics.

(*b*) *Alcohol doping*

It is apparent that impurities dramatically affect the stability and luminescence from SBSL and MBSL. Figure 17 shows the effect of small quantities of alcohols on the luminescence intensity. Note that for a given concentration of alcohol, the intensity diminishes according to the chain length of the alcohol (the vapour pressure of the alcohol decreases with increasing chain length). Similar results are found in MBSL, but with *ca*. 10× the volume concentration of alcohol (Ashokkumar *et al*. 1997). Ashokkumar *et al*. found that if one considers the surface concentration, and not the volume addition, the data appear to group together (a similar grouping occurs in SBSL; figure 17*b*); thus, the surface concentration of the impurity appears to be a dominant factor. Although not shown here, preliminary $R(t)$ curves show that the alcohol has only a small effect on the overall radial motion of the bubble, so that the apparent quenching that is observed does not appear to have an explanation based solely on bubble dynamics. Current work is being conducted to determine whether the quenching is related to the bubble surface, or within the bubble volume.

7. Future perspectives of SBSL

Although each new experiment still results in many new questions, there has been significant progress in the field of SBSL. The pulse width of SBSL can now be measured in many cases. The measured short pulse widths as low as 50 ps suggest focusing of shock waves within the bubble (Moss *et al*. 1997, 1998), leaving open the question of how much stronger the collapse can be made to occur. Consider that for all the known possible fluids, gases and mixtures of fluids and gases, only a very small portion of the available parameter space has been studied. How many other systems can generate stable SBSL? Can current systems be modified to generate stronger collapses (such as introducing an acoustic spike as the bubble collapses)? Some researchers have even suggested that sonoluminescence can occur in neutron stars (Simmons *et al*. 1998)!

At the other end of the scale, the relatively long pulse widths of over 300 ps suggest that it may be possible to make the pulse widths even longer. Do longer pulse widths suggest cooler bubbles? Will line and band emission from such a bubble be observed?

Another mystery of SBSL, the effect of noble-gas doping, appears to have an explanation involving chemical activity of the bubble constituents, the 'microreactor' hypothesis. The robustness of the microreactor hypothesis should be tested by applying the theory to search for other regimes (fluids and gas mixtures) that might yield stable SBSL. Parenthetically, recent evidence of chemical activity from SBSL was found by using the Weissler reaction, where a precipitation of iodide emanated from the vicinity of the sonoluminescence bubble (Lepoint & Lepoint-Mullie 1998).

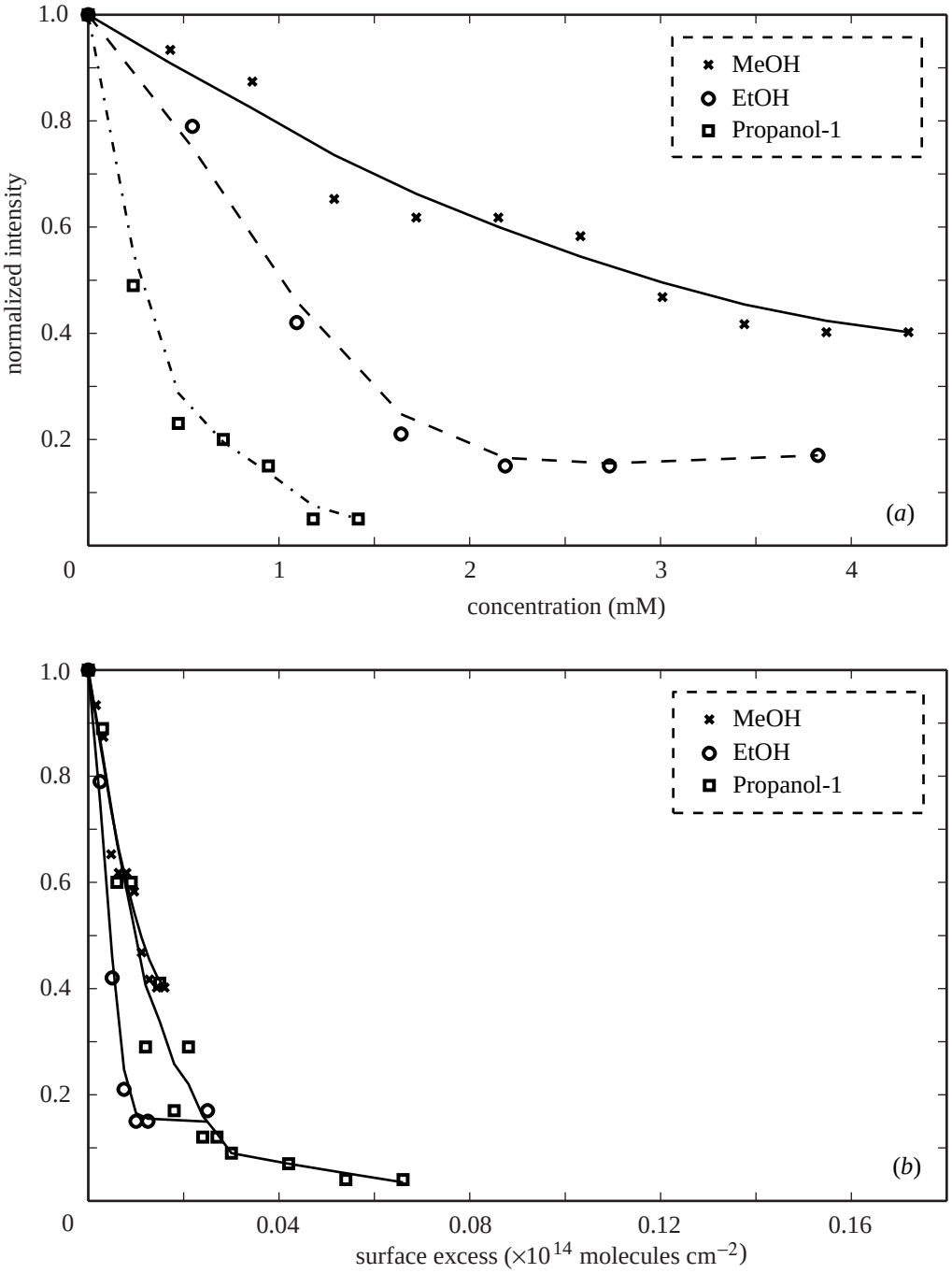

Figure 17. Small quantities of impurities can dramatically affect the intensity from SBSL and MBSL. (*a*) The normalized intensity is plotted as a function of the concentration of the added alcohol. (*b*) The normalized intensity is plotted as a function of the calculated surface excess concentration of the alcohol. (Courtesy of M. Ashokkumar and C. A. Frensley.)

In this paper we have looked at SBSL from the perspective of bubble dynamics, and only explored a small portion of the experiments (and none of the theories) that have recently been published. This intriguing phenomenon should command our attention for many more years. It is our belief that there are still many new and exciting features of sonoluminescence that have yet to be discovered.

The author thanks M. Ashokkumar, L. A. Crum, F. Grieser, and K. S. Suslick for numerous helpful discussions, and M. Ashokkumar, V. Bezzerides, S. M. Cordry, C. A. Frensley, K. Hargreaves and W. B. McNamara III for their help in the laboratory. This research is supported by NSF and DOE.

References

Asaki, T. J. & Marston, P. L. 1994 Acoustic radiation force on a bubble driven above resonance. *J. Acoust. Soc. Am.* **96**, 3096–3099.

Asaki, T. J. & Marston, P. L. 1995 Equilibrium shape of an acoustically levitated bubble driven above resonance. *J. Acoust. Soc. Am.* **97**, 2138–2143.

Ashokkumar, M., Hall, R., Mulvaney, P. & Grieser, F. 1997 Sonoluminescence from aqueous alcohol and surfactant solutions. *J. Phys. Chem.* B **101**, 10 845–10 850.

Barber, B. P. & Putterman, S. J. 1991 Observation of synchronous picosecond sonoluminescence. *Nature* **352**, 318–320.

Barber, B. P., Hiller, R., Arisaka, K., Fetterman, H. & Putterman, S. 1992 Resolving the picosecond characteristics of synchronous sonoluminescence. *J. Acoust. Soc. Am.* **91**, 3061–3063.

Barber, B. P., Hiller, R. A., Löfstedt, R., Putterman, S. J. & Weninger, K. R. 1997 Defining the unknowns of sonoluminescence. *Phys. Rep.* **281**, 66–143.

Cordry, S. M. 1995 Bjerknes forces and temperature effects in single-bubble sonoluminescence. PhD thesis, Department of Physics, University of Mississippi, USA.

Crum, L. A. 1980 Measurements of the growth of air bubbles by rectified diffusion. *J. Acoust. Soc. Am.* **68**, 203–211.

Crum, L. A. & Eller, A. I. 1970 The motion of air bubbles in stationary sound field. *J. Acoust. Soc. Am.* **48**, 181–189.

Crum, L. A. & Prosperetti, A. 1983 Nonlinear oscillations of gas bubbles in liquids: an interpretation of some experimental results. *J. Acoust. Soc. Am.* **73**, 121–127.

Eller, A. I. 1968 Force on a bubble in a standing acoustic wave. *J. Acoust. Soc. Am.* **43**, 170–171.

Engstrom, R. W. 1980 *Photomultiplier handbook*. Princeton, NJ: RCA.

Gompf, B., Gunther, R., Nick, G., Pecha, R. & Eisenmenger, W. 1997 Resolving sonoluminescence pulse width with time-correlated single photon counting. *Phys. Rev. Lett.* **79**, 1405–1408.

Gompf, B., Pecha, R., Nick, G. & Eisenmenger, W. 1998*a* Pulse width and shape in single bubble sonoluminescence. In *16th Int. Congr. on Acoustics and 135th Meeting of the Acoustical Society of America* (ed. P. K. Kuhl & L. A. Crum), pp. 2571–2572. Seattle, WA: Acoustical Society of America.

Gompf, B., Wang, Z. Q., Pecha, R. & Eisenmenger, W. 1998*b* Single bubble sonoluminescence: acoustic emission measurements with a fiber optic probe hydrophone. In *16th Int. Congr. on Acoustics and 135th Meeting of the Acoustical Society of America* (ed. P. K. Kuhl & L. A. Crum), pp. 2849–2830. Seattle, WA: Acoustical Society of America.

Gould, R. K. 1967 Simple method for calibrating small omnidirectional hydrophones. *J. Acoust. Soc. Am.* **43**, 1185–1186.

Hiller, R. A. 1995 The spectrum of single-bubble sonoluminescence. PhD thesis, Department of Physics, Los Angeles, University of California at Los Angeles, USA.

Hiller, R., Putterman, S. & Barber, B. P. 1992 Spectrum of synchronous picosecond sonoluminescence. *Phys. Rev. Lett.* **69**, 1182–1184.

Hiller, R. A., Putterman, S. J. & Weninger, K. R. 1998 Time-resolved spectra of sonoluminescence. *Phys. Rev. Lett.* **80**, 1090–1093.

Holt, R. G. & Gaitan, D. F. 1996 Observation of stability boundaries in the parameter space of single bubble sonoluminescence. *Phys. Rev. Lett.* **77**, 3791–3794.

Holzfuss, J. 1998 Boosting sonoluminescence. *Phys. Rev. Lett.* **81**, 1961–1965.

Ketterling, J. A. & Apfel, R. E. 1998 Sonoluminescence stability for gas saturations down to 0.01 Torr. In *16th Int. Congr. on Acoustics and 135th Meeting of the Acoustical Society of America* (ed. P. K. Kuhl & L. A. Crum), pp. 2839–2840. Seattle, WA: Acoustical Society of America.

Lepoint, T. & Lepoint-Mullie, F. 1998 Single bubble sonochemistry. In *Sonochemistry and sonoluminescence* (ed. L. A. Crum, T. J. Mason, J. L. Reisse & K. S. Suslick), pp. 285–290. London: Kluwer.

Lohse, D., Brenner, M. P., Dupont, T. F., Hilgenfeldt, S. & Johnston, B. 1997 Sonoluminescing air bubbles rectify argon. *Phys. Rev. Lett.* **78**, 1359–1362.

Matula, T. J. & Crum, L. A. 1998 Evidence of gas exchange in single-bubble sonoluminescence. *Phys. Rev. Lett.* **80**, 865–868.

Matula, T. J., Roy, R. A., Mourad, P. D., McNamara, W. B. & Suslick, K. S. 1995 Comparison of multibubble and single-bubble sonoluminescence spectra. *Phys. Rev. Lett.* **75**, 2602–2605.

Matula, T. J., Roy, R. A. & Mourad, P. D. 1996*a* Pulse width of sonoluminescence from cavitation fields. *J. Acoust. Soc. Am.* **101**, 1994–2002.

Matula, T. J., Roy, R. A., Crum, L. A. & Kuhns, D. W. 1996*b* Preliminary experimental observations of the effects of buoyancy on single-bubble sonoluminescence in microgravity and hypergravity. *J. Acoust. Soc. Am.* **100**, 2717.

Matula, T. J., Cordry, S. M., Roy, R. A. & Crum, L. A. 1997*a* Bjerknes force and bubble levitation under single-bubble sonoluminescence conditions. *J. Acoust. Soc. Am.* **102**, 1522–1527.

Matula, T. J., Swalwell, J. E., Bezzerides, V., Hilmo, P., Chittick, M., Crum, L. A., Kuhns, D. K. & Roy, R. A. 1997*b* Single-bubble sonoluminescence in microgravity. *J. Acoust. Soc. Am.* **102**, 3185.

Matula, T. J., Hallaj, I., Cleveland, R. O., Crum, L. A., Moss, W. C. & Roy, R. A. 1998 The acoustic emissions from single-bubble sonoluminescence. *J. Acoust. Soc. Am.* **103**, 1377–1382.

Moss, W. C., Clarke, D. B. & Young, D. A. 1997 Calculated pulse widths and spectra of a single sonoluminescing bubble. *Science* **276**, 1398–1401.

Moss, W. C., Harte, J. A., Levatin, J. L., Rambo, P. W., Young, D. A., Zimmerman, G. B. & Zimmerman, I. H. 1998 Computed spectral and temporal emissions from a sonoluminescing bubble. In *16th Int. Congr. on Acoustics and 135th Meeting of the Acoustical Society of America* (ed. P. K. Kuhl & L. A. Crum), pp. 2843–2844. Seattle, WA: Acoustical Society of America.

O'Connor, D. V. & Phillips, D. 1984 *Time-correlated single photon counting*. London: Academic.

Seghal, C., Sutherland, R. G. & Verrall, R. E. 1980 Selective quenching of species that produce sonoluminescence. *J. Phys. Chem.* **84**, 529–531.

Simmons, W., Learned, J., Pakvasa, S. & Tata, X. 1998 Sonoluminescence in neutron stars. *Phys. Lett.* B **427**, 109–113.

Tian, Y., Ketterling, J. A. & Apfel, R. E. 1996 Direct observation of microbubble oscillations. *J. Acoust. Soc. Am.* **100**, 3976–3978.

PHILOSOPHICAL TRANSACTIONS OF THE ROYAL SOCIETY A MATHEMATICAL, PHYSICAL & ENGINEERING SCIENCES